ACS NANO

www.acsnano.org

ARTICLE

Effect of Electron–Hole Overlap and Exchange Interaction on Exciton Radiative Lifetimes of CdTe/CdSe Heteronanocrystals

Andrés Granados del Águila,[†,‡] Esther Groeneveld,[¶] Jan C. Maan,[‡,†] Celso de Mello Donegá,[¶] and Peter C. M. Christianen[*,†,‡]

[†]High Field Magnet Laboratory (HFML-EMFL), Radboud University, 6525 ED Nijmegen, The Netherlands

[‡]Institute for Molecules and Materials, Radboud University, 6525 AJ Nijmegen, The Netherlands

[¶]Condensed Matter and Interfaces, Debye Institute for Nanomaterials Science, Princetonplein 1, 3584 CC Utrecht, The Netherlands

Supporting Information

ABSTRACT: **Wave function engineering has become a powerful tool to tailor the optical properties of semiconductor colloidal nanocrystals. Core–shell systems allow to design the spatial extent of the electron (e) and hole (h) wave functions in the conduction- and valence bands, respectively. However, tuning the overlap between the e- and h-wave functions not only affects the oscillator strength of the coupled e–h pairs (excitons) that are responsible for the light emission, but also modifies the e–h exchange interaction, leading to an altered excitonic energy spectrum. Here, we present exciton lifetime measurements in a strong magnetic field to determine the strength of the e–h exchange interaction, independently of the e–h overlap that is deduced from lifetime measurements at room temperature. We use a set of CdTe/CdSe core/shell heteronanocrystals in which the electron–hole separation is systematically varied. We are able to unravel the separate effects of e–h overlap and e–h exchange on the exciton lifetimes, and we present a simple model that fully describes the recombination lifetimes of heteronanostructures (HNCs) as a function of core volume, shell volume, temperature, and magnetic fields.**

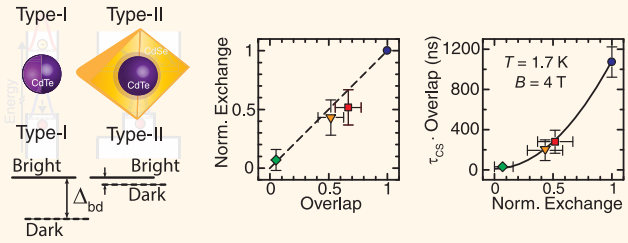

KEYWORDS: *nanocrystals, excitons, core–shell heterostructure, magnetic field, electron–hole exchange, electron–hole overlap*

Quantum mechanical size-confinement of charge carriers in colloidal semiconductor nanocrystals (NCs) leads to optical properties that are fundamentally different from those of the bulk semiconductor material. In particular, the nanoscale localization of the electron- (e-) and hole- (h-) wave functions leads to an enhanced e–h exchange interaction (η) that lifts the spin degeneracy of the exciton energy levels and produces fine structure. The e–h exchange-induced energy splitting leads to a characteristic temperature dependence of the radiative lifetime of the electron–hole (exciton) recombination: at room temperature (RT), the lifetime is short (~10 ns), because emission originates from an optically active state (the bright state). At low temperature (LT, $T < 4$ K), the emission decay time is much longer (~1 μs), because the lowest exciton level, just below the bright state is optically passive (the so-called dark state).[1−4] The energy separation Δ_{bd} between the bright and dark exciton states scales with the exchange interaction as $\Delta_{bd} = 3\eta \propto 1/R^3$, where R is the NC radius.[1,5,6] For CdSe NCs, Δ_{bd} ranges from ~20 meV for $R \sim 1$ nm to ~2 meV for $R \sim 2.5$ nm.[7] Alternatively, the e–h exchange energy can be controlled by wave function engineering. Recently, it has been shown that the spatial extent of the wave functions of electrons- (ψ_e) and holes (ψ_h) can be separately tuned by using core–shell heteronanostructures (HNCs). HNCs combine two semiconductor materials with different bandgap values and, most importantly, different offsets for the conduction and valence bands, which allows to vary the spatial overlap between ψ_e and ψ_h. In type-I NCs, both electrons and holes are confined to the core, leading to a large e–h overlap (left panel Figure 1a). In type-II HNCs, the electrons and holes are spatially separated (spatially indirect excitons), reducing the e–h overlap (right panel Figure 1a). In the intermediate case, which is referred to as type-I$^{1/2}$ or quasi-type-II (middle panel Figure 1a), one type of carrier is confined to the core, whereas the other type is delocalized over the core–shell or *vice versa*. Changing the overlap of the electrons and holes strongly modifies the exciton radiative lifetimes and its temperature dependence.[8−15] However, two competing effects can be distinguished. With

Received: November 13, 2015
Accepted: March 16, 2016
Published: March 16, 2016

DOI: 10.1021/acsnano.5b07158
ACS Nano 2016, 10, 4102–4110

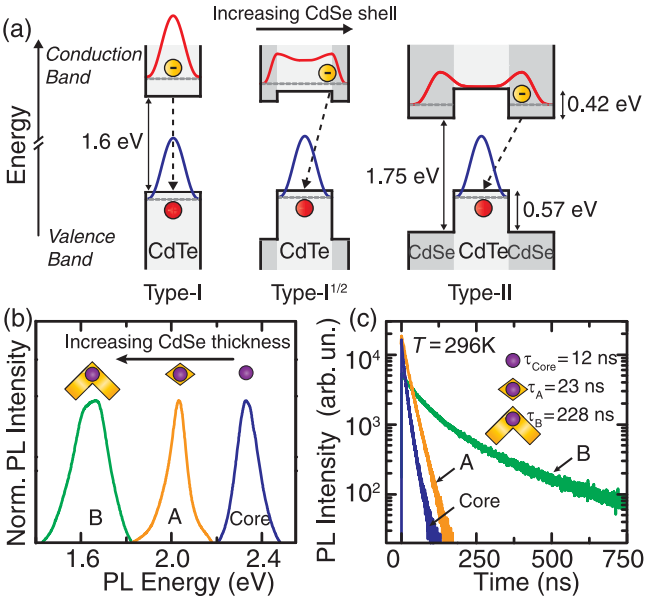

Figure 1. Sample description and characterization. (a) Schematic representation of the three band alignment regimes in CdTe/CdSe core−shell heteronanostructures (HNCs). The bulk bandgap values and the conduction and valence band-offsets of CdTe and CdSe are indicated.[16] Core-only structures display the regular type-I band-alignment (left panel) with a large overlap of the electron (red solid curve) and hole (blue solid curve) wave functions. In the type-I$^{1/2}$ band-alignment configuration (middle panel), the hole wave function is confined to the CdTe core, whereas the electron wave function is delocalized over the core−shell, decreasing the e−h overlap. In type-II structures, the electron and hole are spatially separated (right panel). Dashed arrows indicate the optical recombination pathways. (b) Normalized PL spectra of the core-only (blue curve), HNC-A (orange curve), and HNC-B (green curve) samples, obtained at 4.2 K with 2.6 eV excitation energy. The PL peak energy progressively shifts to lower values with increasing shell volume. (c) Room temperature (296 K) PL decay curves (excitation energy 3.06 eV) on a semilogarithmic scale using the color-code of (b). The PL decay becomes longer with increasing shell volume.

decreasing e−h overlap, the oscillator strength of excitonic recombination will decrease, leading to *longer* exciton lifetimes, both at high and low temperatures. In contrast, a reduced e−h overlap will result in a lower e−h exchange energy and concomitantly a smaller Δ_{bd}. It has been proven that a reduced Δ_{bd} leads to a *shorter* exciton lifetime at low temperatures and a drastic change in its temperature dependence.[12] It is, therefore, of crucial importance to independently determine the e−h overlap and the e−h exchange energy to understand the exciton recombination rates of HNCs. In this paper, we demonstrate that it is possible to obtain the e−h exchange interaction energy by measuring the photoluminescence (PL) decay times in a very strong applied magnetic field (B). We combine these values with those of the e−h overlap determined from the RT exciton lifetime to obtain a thorough understanding of the exciton recombination rates.

For our studies, we use a set of four CdTe/CdSe HNCs, where we systematically vary the CdSe shell volume to control the extensions of ψ_e and ψ_h. The band-alignment of the CdTe/CdSe interface[16] is such that ψ_h is always localized within the CdTe core, whereas ψ_e shifts from the core (CdTe core without shell) toward the CdSe region with increasing shell volume (see Figure 1a).[8,11] This transition is monitored by detailed PL decay measurements as a function of magnetic field strength and temperature. For the core-only CdTe sample, we find the typical behavior for type-I NC. The lifetime shortens dramatically with temperature, as described above. The low temperature (dark exciton) PL decay time becomes much smaller with increasing field strength, because of the field induced mixing between dark and bright excitons.[5,7,17−20] Since the bright−dark mixing depends on the ratio between the Zeeman and e−h exchange energies, η can be determined from the field dependent lifetimes. The sample with the thickest CdSe shell shows a completely different behavior, namely a lifetime that is almost independent of temperature and magnetic field, which is due to a vanishing exchange energy for such a type-II nanostructure. Our results show that both the e−h overlap and the e−h exchange energy progressively decrease with increasing shell volume. These findings allow us to disentangle the effects on the exciton lifetime of both e−h overlap and exchange energy and to formulate a simple model that quantitatively describes the exciton lifetime as a function of core size, shell volume, temperature, and magnetic field strength. This formula is applicable to HNCs of other material systems as well.

RESULTS AND DISCUSSION

Sample Characterization and Optical Properties. A set of high-quality colloidal CdTe/CdSe HNCs were synthesized using the seeded growth methodology.[8,11] Nearly spherical CdTe cores were prepared with radius R = 1.3 nm (10% size dispersion) and volume (V_{HNC}) = 9.2 nm^3. These cores were overgrown with CdSe shells with anisotropic shapes and variable thicknesses: sample HNC-A has total volume V_{HNC} = 15 nm^3 with V_{CdSe} = ∼5.8 nm^3, and sample HNC-B has total V_{HNC} = 80 nm^3 with V_{CdSe} = ∼70.8 nm^3. These samples have been extensively characterized by X-ray diffraction, high-resolution transmission electron microscopy, and optical spectroscopy.[8,10] The CdTe core sample was found to exhibit a zinc blende structure, whereas the HNC samples all have shown only the wurtzite structure, even for HNCs with relatively thin CdSe shells (such as HNC-A with 39% CdSe volume fraction). No evidence for polytypism has been found. A third HNC (HNC-C) with core radius R = 1.45 nm with total volume V_{HNC} = 18 nm^3 and V_{CdSe} = ∼5.2 nm^3 was also investigated. The core (10% size dispersion) of HNC-C exhibits identical optical properties to that of HNC-A and HNC-B with equivalent PL emission energy and radiative lifetimes. For the optical experiments, regular drop-casted samples were prepared in which the HNC ensembles are randomly oriented. Steady-state photoluminescence PL and time-resolved photoluminescence (trPL) were performed as a function of temperature and applied magnetic field (see Methods section). We have confirmed that the measurements on drop-casted samples are in good agreement with those in cuvettes (frozen solutions), meaning that we can safely neglect effects of energy transfer.

Figure 1 shows the low-temperature steady-state PL spectra (b) and the room temperature PL decay transients (c) of the core-only, HNC-A, and HNC-B samples. Figure S1 shows the corresponding data for HNC-C. With increasing CdSe shell volume, the PL spectral position shifts to lower energies, relative to the green PL of the core (2.32 eV; 535 nm). The largest spectral shift was observed for the thickest shell sample (HNC-B) with its emission in the near-infrared region (1.65 eV; 750 nm), below the bulk band gap energy of CdSe (1.75

DOI: 10.1021/acsnano.5b07158
ACS Nano 2016, 10, 4102−4110

eV) and close to the bulk bandgap of CdTe (1.6 eV). The room temperature PL decay times become substantially longer with increasing shell volume (Figure 1c). The extracted exciton lifetimes monotonically increase from a value of 12 ± 2 ns for the core, to 228 ± 10 ns for HNC-B. These spectroscopic signatures evidence the transition from type-I core samples to type-II HNCs with spatially indirect excitons, with a long RT lifetime and a PL emission energy close to the CdTe bandgap (Figure 1a).[8,10]

Temperature Dependence of the Exciton Lifetimes. Figure 2 shows the PL decay curves of samples HNC-A (a) and HNC-B (b) at selected temperatures between 1.7 and 296 K. Figure S2 shows the temperature dependence of the integrated PL intensity of samples HNC-A and HNC-B, showing a roughly constant intensity. The transients were recorded at the maximum of the PL emission using pulsed laser excitation at 3.06 eV. HNC-A (Figure 2a) shows a PL decay time that drastically decreases with temperature, qualitatively similar to previous reports for CdSe and CdTe type-I QDs.[2,3,20] In contrast, the PL decay curves of HNC-B are remarkably independent of T. HNC-A manifests single-exponential decays at elevated temperatures (T > 20 K), while in the low-temperature regime, the trPL traces show a biexponential decay with a fast and a slow channel. HNC-B shows biexponential decay in the entire temperature range. A full discussion of the origin of the multiexponential decay, and how it depends on temperature, is beyond the scope of this work and has been presented elsewhere.[10] Here we focus our attention on the slow decay time, which reflects the radiative lifetime of long-lived excitons emitted from the lowest-energy exciton state. The PL decay times (τ_{cs}) are obtained by analyzing the end part of the decay curves (last 5−10% of the initial intensity at t = 0) using a single-exponential fit, which is a common procedure in the determination of the exciton lifetimes in colloidal semiconductor nanocrystals.[2,20]

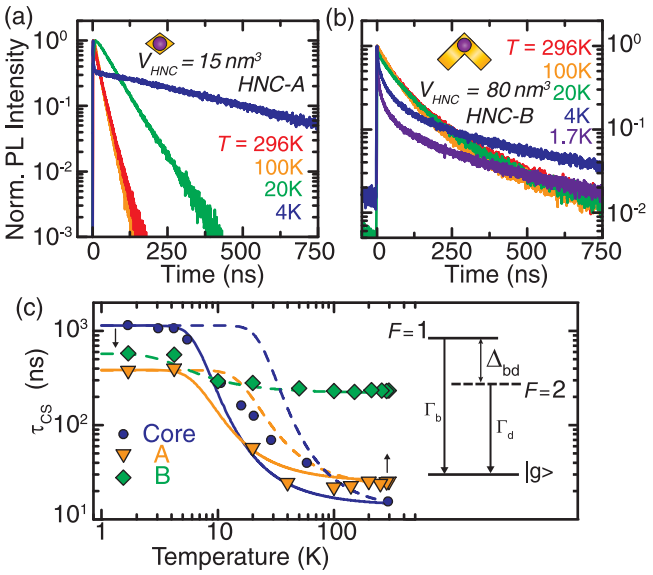

Figure 2. PL decay as a function of temperature. Normalized PL decays of samples HNC-A (a) and HNC-B (b) at selected temperatures on a semilogarithmic scale. The signal was measured at the center of the PL spectra using 3.06 eV excitation energy. (c) Temperature-dependence of the exciton lifetimes of the CdTe core (blue circles), HNC-A (orange down-triangles) and HNC-B (green diamonds) samples. Symbol sizes are larger than or comparable to the experimental errors. Dashed-lines are fits to the data with $\Delta = \Delta_{bd}$ by using eq 3. Solid-lines are best fits to the data with the same model but varying $\Delta(\neq \Delta_{bd})$ (see text). (Inset) Three-level energy scheme: $|g\rangle$ is the ground-state, F = 1 and F = 2 are the lowest-energy bright and dark levels with radiative recombination rates Γ_b and Γ_d, respectively. Δ_{bd} is the energy separation between the two exciton states.

The T-dependence of the extracted lifetimes of the CdTe-core (blue-circles), HNC-A (orange down-triangles), and HNC-B (green-diamonds) samples is reported in Figure 2c. Surprisingly, the CdTe core-only sample exhibits the regular behavior for a type-I wurtzite nanocrystal, despite the fact that it has a zinc blende crystal structure. However, this is consistent with the results of previous temperature and magnetic field dependent exciton PL decay time experiments on CdTe nanocrystals.[20,21] We attribute this behavior to a nonspherical shape of the zinc blende CdTe cores, resulting in a wurtzite-type response. In the remainder of the paper, we will, therefore, only consider a wurtzite-type exciton band structure characterized by the bright−dark exciton level diagram schematically depicted as inset in Figure 2c. In this model, the exciton states are labeled by the projection of the angular momentum (F) on the c-axis of a wurtzite NC. At high temperatures, when the thermal energy (k_BT) is larger than the energy separation Δ_{bd} between the dark and bright excitons, the PL emission originates from the high-oscillator strength (bright) exciton state ($|F|$ = 1), yielding a short decay time. At low temperatures ($k_BT < \Delta$), light emission arises from the low-oscillator strength (dark) exciton state ($|F|$ = 2), characterized by a very long lifetime reaching an intriguing constant (plateau) value at temperatures below 4.2 K.[2,3] This typical T-dependence gradually disappears with increasing CdSe shell volume and is nearly absent for HNC-B, which proves that the response of type-II HNCs is entirely different from that of type-I nanocrystals. A similar temperature-behavior has been shown for quasi-type-II core/shell CdSe/CdS HNCs.[12]

Magnetic Field Dependence of the PL Decay Times. Figure 3 shows PL decay curves at selected B-fields for the core only (a) and HNC-B (b) samples (see Figure S1 for data on HNC-C). The samples display a remarkably different behavior: the PL decay time of the core-only sample drastically decreases with increasing field, whereas the PL transients of sample HNC-B do not depend on field strength at all. The full field dependencies of the extracted PL decay times of all four samples are depicted in Figure 3c. The CdTe-core lifetime shortens significantly with field to 450 ± 50 ns, which is ∼60% of the zero-field lifetime (1.14 ± 0.05 μs). This behavior is typical for type-I CdSe[7,17,18] and CdTe[20,21] nanocrystals. The PL decay times of samples HNC-A and HNC-C show only a modest reduction with field (to ∼30% of the zero field lifetime). Most importantly, the PL lifetime of HNC-B is constant (∼570 ns) up to the highest field strength used (28 T).

Determination of the Electron−Hole Overlap. At room temperature (T = 296 K), the PL decay times τ_{cs} increase with V_{CdSe} from 12 ± 2 ns for the core (V_{CdSe} = 0 nm³) to 228 ± 10 ns for HNC-B (V_{CdSe} = 70.8 nm³) (Figures 1c and 2c). At such high temperatures, the decay times are determined by the lifetime of bright excitons, without contribution from the dark exciton level. The significant increase of the RT PL lifetime with increasing shell-thickness indicates that the oscillator-strength of the bright exciton transition decreases. These changes are caused by the (partial) spatial separation of ψ_e and

DOI: 10.1021/acsnano.5b07158
ACS Nano 2016, 10, 4102−4110

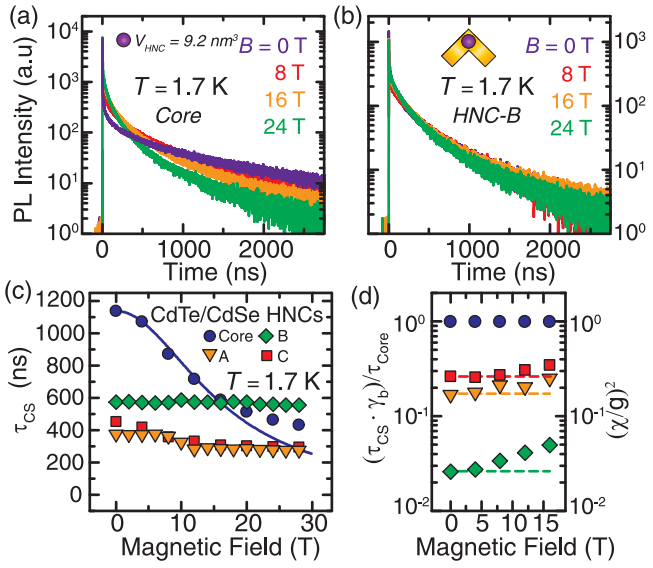

Figure 3. Magnetic field dependence of the PL decay times. Low-temperature (1.7 K) PL decay curves of CdTe core-only (a) and HNC-B (b) samples at applied magnetic fields of 0 (violet curves), 8 (red curves), 16 (orange curves), and 24 T (green curves). (c) Magnetic-field evolution of the extracted LT PL lifetimes τ_{cs} for core-only (blue circles), HNC-A (orange down-triangles), HNC-B (green diamonds), and HNC-C (red squares) samples. Symbol sizes are larger than or comparable to the experimental errors. The blue solid curve is calculated with eq 1. (d) Magnetic field dependence of the experimental PL lifetimes τ_{cs} normalized to the core-lifetime τ_{core} and the ratio γ_b of the bright exciton lifetimes of HNC and core-only samples. The symbols are the same as in (c), with sizes that are larger than or comparable to the experimental errors. The dashed-lines are best fits of the data to eq 2.

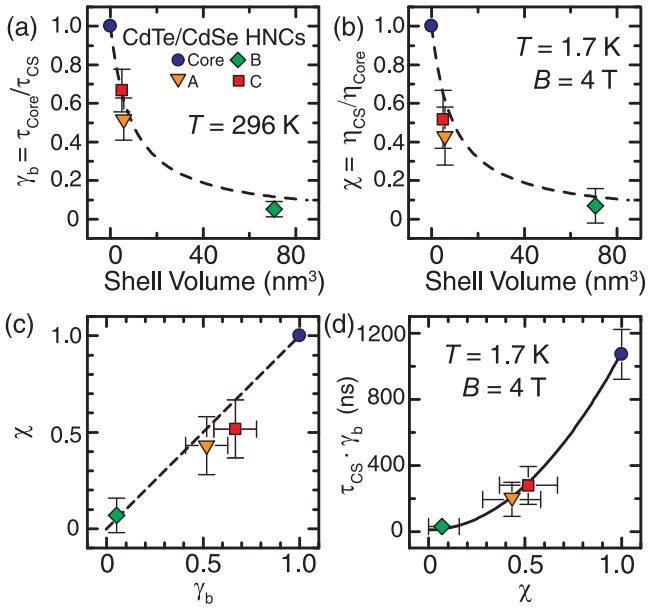

Figure 4. Electron–hole overlap and exchange interaction. (a) Values of $\gamma_b = \tau_{core}^{RT}/\tau_{cs}^{RT}$ extracted from the room temperature PL lifetimes as a function of the HNC-shell volume for the CdTe-core (blue circles), HNC-A (orange down-triangles), HNC-B (green diamonds), and HNC-C (red squares) samples. The same symbols- and color-codes are used in all panels. (b) Values of the normalized exchange energy $\chi = \eta_{cs}/\eta_{core}$ obtained from the magnetic field dependence of the low-temperature PL lifetimes, as a function of the HNC-shell volume. (c) χ *versus* γ_b using the experimental values of (a) and (b). Notice the nearly linear relationship between χ and γ_b. The dashed lines in (a–c) are guides for the eye. (d) The effective lifetime $\tau_{cs} \cdot \gamma_b$ as a function of χ at 1.7 K and at 4 T. The black line is calculated using eq 4.

ψ_h (see Figure 1a), resulting in a decreased e–h overlap integral (squared) defined as $\Theta_{e-h} = |\int \psi_e^*(r)\psi_h(r)\, dV|^2$ over the HNC volume. The radiative decay rate Γ_b ($\tau_b = 1/\Gamma_b$) of the optically active excitons is directly proportional to Θ_{e-h}.[22,23] Therefore, the ratio of the room temperature lifetimes of the core-only and HNC samples, expressed by the dimensionless parameter $\gamma_b = \tau_{core}^{RT}/\tau_{cs}^{RT}$ can be used to quantify the overlap of ψ_e and ψ_h (see Figure S3). The dielectric constant (ϵ) and the refractive index ($n^2 = \epsilon$) contribution to γ_b can be safely neglected, since for CdTe and CdSe both parameters are very similar ($\epsilon_{CdTe} = 9$ and $\epsilon_{CdSe} = 7.8$).[22]

The experimental values of γ_b are shown in Figure 4a as a function of the HNC CdSe shell-volume. By definition, $\gamma_b = 1$ for the core-only sample. It decreases with increasing V_{HNC} to 0.5 ± 0.1 for HNC-A and 0.05 ± 0.02 for HNC-B. The same methodology has been used to estimate the e–h overlap for quasi-type-II CdSe/CdS HNCs.[12,24] We notice here, however, that for those CdSe/CdS quasi-type-II HNCs, γ_b does not strictly follow a linear dependence with the PL emission energy for all CdS-shell dimensions, as in the case of the truly type-II CdTe/CdSe HNCs studied here (see Figure S3). For type-II HNCs, changes in the spatial distribution of the electronic-wave functions results in a continuous change in both the optical transition energy and the RT radiative decay rate (see Figure 1a,c and Figure S3) with increasing the HNC shell-volume. These are clear spectroscopic signatures of the formation of spatially indirect excitons.

At the lowest temperature (T = 1.7 K), the PL decay time is dominated by the dark exciton lifetime, which is very long for the core-only sample (1.14 ± 0.05 μs). However, with increasing V_{HNC}, the lifetime decreases to 380 ± 50 ns for HNC-A to increase again to 570 ± 50 ns for HNC-B. This nonmonotonic dependence of the PL decay time on V_{HNC} points to two competing effects. On one hand, the reduced e–h overlap leads to a diminishing oscillator strength and thus longer decay times. On the other hand, it leads to a decrease in the exchange interaction, resulting in a lowering of the bright–dark splitting. Regular type-I HNCs with small (large) Δ_{bd} shows faster (longer) LT PL lifetimes.[3,20] Therefore, any reduction in the exchange coupling leads to shorter decay times. Without the separate determination of the effects of the electron–hole overlap and the electron–hole exchange interaction, it is very difficult to fully understand exciton dynamics in semiconductor nanocrystals.

Determination of the Electron–Hole Exchange Energy: *g*-Factor Approximation. Within the effective-mass-approximation (EMA), radiative recombination of the dark exciton is strictly forbidden[5] and size-independent. Only in the presence of a strong magnetic field the dark exciton acquires oscillator strength due to field-induced mixing between the bright and dark excitons, which occurs for a wurtzite nanocrystal whose *c*-axis makes an angle (θ) with the direction of the *B*-field. As a result, the PL decay time of quasi-spherical type-I nanocrystals drastically reduces with increasing field strength (core-only sample in Figure 3c), in agreement with literature.[12,17,18,20,25] Quantitatively, the degree of exciton mixing scales with $\zeta = E_z/3\eta$, the ratio of the Zeeman energy $E_z = \mu_B g_e B$ (μ_B is the Bohr magneton and g_e is the electron *g*-

DOI: 10.1021/acsnano.5b07158
ACS Nano 2016, 10, 4102–4110

factor) and the bright−dark splitting ($\Delta_{bd} = 3\eta$, with η the e−h exchange energy), leading to a field-dependent exciton lifetime:[5]

$$\frac{1}{\tau(B,\theta)} = \frac{\sqrt{1+\zeta^2+2\zeta\cos\theta} - 1 - \zeta\cos\theta}{\sqrt{1+\zeta^2+2\zeta\cos\theta}} \frac{3}{4\tau_b} \quad (1)$$

The solid blue curve in Figure 3c is a fit to the core-only data following the procedure described in ref 20. In this calculation, we used the following parameters: $\tau_{core}^{LT} = 1.14\ \mu s$, the low temperature lifetime at $B = 0$ to start with the proper value at zero field.[20] $\tau_b = \frac{1}{2}\tau_{core}^{RT} = 6$ ns; the bright exciton lifetime is half the room temperature PL decay time. The factor (1/2) accounts for the correct implementation of the room temperature decay time in the model described later on. For the electron g-factor, a value of $|g_e| \simeq 1.7$ is used, which is equal to the bulk CdTe electron g-factor and to the value calculated for a CdSe QD with a size comparable to our CdTe core.[26] Finally, η is used as the only fitting parameter. We obtain $\eta = 5.0 \pm 0.5$ meV and $\Delta_{bd} = 15.0 \pm 1.5$ meV, leading to acceptable fits to the experimental data, especially at low and intermediate fields. The reason why the calculated lifetimes at high fields underestimate the experimental ones is not clear, but this does not hamper the determination of the exchange energy based upon the low field regime. The resulting values are in approximate agreement with the zero-phonon line energies obtained for CdTe QDs.[27] The field-dependent dark exciton lifetimes thus gives direct access to the value of the exchange energy in colloidal dots. In the following, we will use this dependence to determine the exchange energy of HNCs when the lifetimes are also affected by the reduced e−h overlap.

In the limit of weak magnetic fields, the orientation-averaged dark exciton decay rate Γ_d is proportional to $\frac{1}{2}\zeta^2/\tau_b$.[5] We can use the field-dependent LT decay times of the core-only sample ($\tau_{core}^{LT}(B)$) as a normalization to the lifetimes of the CdTe/CdSe HNCs ($\tau_{cs}^{LT}(B)$) by introducing a dimensionless parameter $\gamma_d = \tau_{core}^{LT}(B)/\tau_{cs}^{LT}(B)$ resulting in

$$\gamma_d = \frac{\tau_{core}^{LT}}{\tau_{cs}^{LT}} = \frac{\tau_{core}^{RT}}{\tau_{cs}^{RT}}\left(\frac{g}{\chi}\right)^2 = \gamma_b\left(\frac{g}{\chi}\right)^2 \quad (2)$$

where $g = g_{cs}/g_{core}$ corresponds to the normalized Zeeman energy given by the ratio of the g-factors and $\chi = \eta_{cs}/\eta_{core}$ is the normalized exchange energy. In Figure 3d, we show the experimental values of the ratio γ_b/γ_d between 0 and 16 T for all samples. At low fields, all samples exhibit a roughly constant γ_b/γ_d value: HNC-A and -C up to 10 T, while HNC-B shows only a rather modest increase with B-field. This result shows that the field-independent normalization (eq 2) works very well for these samples and even extends to zero field.

This is surprising in the framework of the effective mass approximation, because, first, eq 2 is not valid at zero field because in the dipole-approximation radiative recombination of the dark exciton is strictly forbidden and the exciton lifetime goes to infinity. Finite dark exciton lifetimes are, however, experimentally reported for a number of different colloidal nanocrystal systems (CdSe, CdTe, InAs, PbSe, and ZnSe),[1−3,21,25,28−30] and computed by semiempirical tight-binding[31] and pseudopotential[32] calculations. Such a measurable dark recombination time highlights the limitation of the EMA at zero magnetic field. Second, eq 2 is derived for type-I nanocrystals, whereas here it is applied to type-II HNCs. Most strikingly, γ_b/γ_d at low fields (indicated by the dashed lines in Figure 3d) strongly varies with sample from $\gamma_b/\gamma_d = 1$ for the core-only, to $\gamma_b/\gamma_d = 0.18 \pm 0.02$ and 0.26 ± 0.03 for samples HNC-A and HNC-C, respectively, and $\gamma_b/\gamma_d = 0.027 \pm 0.002$ for sample HNC-B. The orders of magnitude variation in $\gamma_b/\gamma_d = (\chi/g)^2$ with increasing NC volume is mainly due to the reduction in χ, *i.e.*, the exchange energy of HNCs relative to that of the core, because we can safely assume that the variation in the g-factor among the samples is much smaller (see below).

Detailed experimental values for the g-factors of electrons, holes, and excitons in colloidal QDs, as a function of size and composition (shell structure), are not available, and in particular, data for CdTe QDs is scarce.[20,21] To calculate the g-factor in a HNC is rather complex, because it depends on the size-confinement, internal/shape anisotropy,[33] and surface contributions,[34,35] where the core/shell interface details becomes important, as well as interfacial strain.[36] However, neglecting interfacial effects, the effective g-factor can be written as $\langle g_{cs}\rangle = \langle g_{core}\rangle + \langle g_{shell}\rangle$[34−36] as the sum of the weighted volume contributions of each material to account for the penetration of ψ_e into the surrounding shell.

Considering that the ratio between the core (V_{core}) and the total HNC (V_{HNC}) volume is described by the dimensionless parameter x ($x = V_{core}/V_{HNC}$), the core/shell g_{cs}-factors can be written as $\langle g_{cs}\rangle = g_{core}x + g_{shell}(1-x)$. In the former expression, $x \approx 1$ corresponds to the situation when the shell-volume is negligible as compared to the core ($V_{HNC} \approx V_{core}$), while $x \approx 0$ denotes a large shell-volume ($V_{HNC} \approx V_{shell}$), since $V_{HNC} = V_{core} + V_{shell}$. In this approach, we use the bulk g-factor of the core material ($|\langle g_{cs}\rangle| \approx |\langle g_{core}\rangle| = 1.67$ (CdTe)) for the thin-shell HNCs (HNC-A, HNC-C),[37] whereas for sample HNC-B, we take the bulk g-factor of the shell material ($|\langle g_{cs}\rangle| \approx |\langle g_{shell}\rangle| = 0.68$ (CdSe)). These values are consistent with the analysis of the PL decay times at high magnetic fields (see below, Figure S4 and Supporting Discussion). Furthermore, because we use a dimensionless analysis, dividing all parameters of the HNC samples by those of the core, the outcome of the model is not very sensitive to small variations in the actual g-factor values. As a result, this analysis directly allows us to obtain values for the normalized exchange energy $\chi = \eta_{cs}/\eta_{core}$ (Figure 4b). χ shows a monotonic reduction with CdSe-shell volume from 0.43 ± 0.14 (HNC-A) and 0.52 ± 0.15 (HNC-C) to 0.07 ± 0.08 for the biggest CdSe-shell sample HNC-B. Inserting the fitted $\eta_{core} = 5.0 \pm 0.5$ meV for the CdTe-core, we obtain $\eta_{cs} = 2.1 \pm 0.8$, 0.3 ± 0.3, and 2.6 ± 0.8 meV for samples HNC-A, -B, and -C, respectively. Measuring the magnetic dependence of the PL decay times, therefore, provides an independent measure of the exchange interaction in semiconductor nanocrystals.

The symbols in Figure 4c show the relationship between the two independently determined parameters, the normalized exchange energy χ, and the e−h overlap represented here by γ_b. The electron−hole exchange coupling ($\propto \chi_{exch} = \int|\psi_e(r)|^2|\psi_h(r)|^2\ dV$) is found to be linearly proportional to the e−h overlap ($|\int\psi_e^*(r)\psi_h(r)\ dV|^2$). This linear trend is in excellent agreement with recent effective-mass calculations for quasi-type-II quasi-spherical CdSe/CdS HNCs[12] and has been previously used to explain the variable hole spin relaxation times in nearly spherical type-II CdTe/CdSe NCs.[38] Our results show that also in the case of nonspherical type-II CdTe/CdSe HNCs $\chi \sim \gamma_b$.

Electron−Hole Exchange, Electron−Hole Overlap, and Exciton Lifetimes. The starting point in the derivation of the expression of the exciton decay rate Γ_{cs}, including e−h overlap

DOI: 10.1021/acsnano.5b07158
ACS Nano 2016, 10, 4102−4110

and exchange interaction of HNCs, is the dark−bright exciton level scheme (Figure 2c):

$$\Gamma_{cs} = \tau_{cs}^{-1} = [\Gamma_d^{cs} + \Gamma_b^{cs} e^{-(\Delta/k_B T)}][1 + e^{-(\Delta/k_B T)}]^{-1}$$

This model assumes thermal equilibrium between two exciton levels separated by an energy $\Delta = \Delta_{bd}$. The decay rates are $\Gamma_d^{cs} = \frac{1}{\tau_d^{cs}}$ and $\Gamma_b^{cs} = \frac{1}{\tau_b^{cs}}$ for the dark and bright levels, respectively. The low temperature ($k_B T \ll \Delta$) and high temperature ($k_B T \gg \Delta$) limits of the model are given by, respectively, $\Gamma_{cs} \sim \Gamma_d^{cs}$ and $\Gamma_{cs} \sim \frac{1}{2}\Gamma_b^{cs}$. Combining this with the definitions of $\gamma_b = \tau_{core}^{RT}/\tau_{cs}^{RT}$ and $\gamma_d = \tau_{core}^{LT}(B)/\tau_{cs}^{LT}(B)$, we find that $\Gamma_b^{cs} = 2/\tau_{cs}^{RT} = 2\,\gamma_b/\tau_{core}^{RT}$ and $\Gamma_d^{cs} = \gamma_b(g/\chi)^2/\tau_{core}(B)$. Here we have incorporated the magnetic-field dependence of the low-temperature PL decay time *via* $\Gamma_d^{cs} = \frac{1}{\tau_d^{cs}(B)}$. Finally, as described above, we can neglect the influence of the *g*-factor on the lifetime at zero fields: $\Gamma_d \sim \gamma_b/\chi^2 \cdot \tau_{core}^{LT}(B)$, yielding

$$\Gamma_{cs} = \frac{1}{\tau_{cs}} = [\frac{\gamma_b}{\chi^2 \tau_{core}^{LT}(B)} + \frac{2\gamma_b}{\tau_{core}^{RT}} e^{-(\Delta/k_B T)}][1 + e^{-(\Delta/k_B T)}]^{-1} \quad (3)$$

The observed exciton lifetime depends on a number of parameters: (1) The lifetimes of the dark (τ_{core}^{LT}) and bright exciton (τ_{core}^{RT}) levels, experimentally determined by measuring the PL decay time of the core-only sample at, respectively, low temperature and room temperature. (2) The energy splitting Δ, which creates a characteristic temperature dependence. (3) The e−h overlap (expressed by γ_b), which means that a reduced overlap leads to a longer PL decay time. (4) The exchange energy (expressed by χ), leading to longer low-temperature lifetimes with increasing exchange energy. (5) The magnetic field induced bright−dark exciton mixing through $\tau_{core}^{LT}(B)$.

This bright−dark model is an example of a classical 3-level model (inset of Figure 2c). The model takes into account only one bright state, irrespective of the bright−dark splitting, temperature, and electron−hole overlap. We neglect the influence of any additional higher energy bright exciton level (for instance, at high T or small Δ_{bd}), assuming that the relaxation from the higher exciton levels to the lowest dark one is sufficiently fast to equilibrate the levels. The biexponential decays of samples HNC-A and HNC-B at elevated temperatures[10] suggest that this approximation may not be completely valid at these temperatures, resulting in deviations from the behavior predicted by the model. Furthermore, we assume that this exciton fine-structure works equally well for both direct and indirect excitons (Type-I and type-II NCs). Finally, any effect of phonon-assisted recombination is ignored. Essentially, this expression is a modification of the formula given by Brovelli *et al.*[12] with two additional ingredients (exchange energy and magnetic field dependent dark exciton recombination rate Γ_d) to capture the main characteristics of the behavior of the PL decay transient. As shown in the following, this allows a quantitative description of the exciton lifetime as a function of experimental parameters: temperature, magnetic field, core size, and shell volume.

Dark Exciton Lifetimes. In the limit of low temperatures, the PL lifetime (τ_{cs}^{LT}) is entirely determined by the dark exciton level. To disentangle the effect of the e−h overlap from that of the exchange interaction, we divide eq 3 by γ_b, and define an effective dark exciton lifetime as

$$\tau_{cs}^{LT} \cdot \gamma_b \simeq \tau_{core}^{LT} \cdot \chi^2 \quad (4)$$

to study the isolated effect of the exchange interaction (χ). Figure 4d shows $\tau_{cs}^{LT}\gamma_b$ (4 T, 1.7 K) as a function of χ for all samples measured. The effective lifetime monotonously increases with increasing χ from 30 ns for HNC-B to 200, 300, and 1071 ns for samples HNC-C, HNC-A, and CdTe-core, respectively. Indeed, it scales quadratically with χ as indicated by the solid line, in agreement with eq 4. In this case, the exchange interaction energy is modified by reducing the overlap between the electron and hole wave functions of the dark exciton. Alternatively, the exchange interaction can be varied by changing the diameter of spherical NCs ($\eta \propto 1/R^3$). Indeed, regular type-I NCs[3,25,39] exhibit longer (shorter) lifetimes at $T \leq 4.2$ K with decreasing (increasing) NC size (see Figure S5 and Supporting Discussion). Zero-field mixing between bright and dark excitons levels have been proposed to account for this size dependence, where the degree of mixing would scale inversely proportional to the bright−dark energy splitting,[3,40] with the former being proportional to the exchange energy $\Delta_{bd} \propto \eta$. Our results demonstrate the universal effect of the exchange energy on the (effective) dark exciton lifetime (eq 4), irrespective of whether η is varied by size or e−h overlap.

***B*-Dependence of the Dark Exciton Lifetimes.** Figure 5a summarizes the experimental data of Figure 3c by plotting the effective lifetime $\tau_{cs}^{LT}\cdot\gamma_b$ for all samples (see Figure S6 for a logscale plot). The solid blue line corresponds to eq 1 with η = 5 meV, g_e = 1.7, τ_{core}^{LT} = 1.14 μs, $\tau_b = \frac{1}{2}\tau_{core}^{RT}$ = 6 ns (see also solid blue line in Figure 3c). Inserting this field-dependent $\tau_{core}^{LT}(B)$, the experimental values of γ_b and χ, and g_e = 1.7 (HNC-A, HNC-C) and g_e = 0.7 (HNC-B) in eq 3 leads to the solid lines in Figure 5. The agreement between calculated values and the experimental data is very satisfactory, and the main features of the data are well described. For the core-only

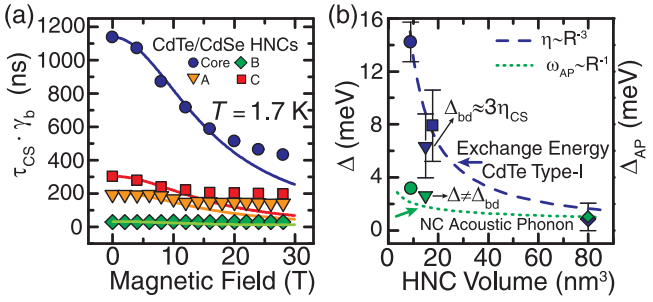

Figure 5. Bright−dark splitting *versus* acoustic phonon energy: determination of Δ in eq 3. (a) Magnetic-field dependence of the LT effective exciton lifetimes ($\tau_{cs}\cdot\gamma_b$) for core-only (blue circles), HNC-A (orange down-triangles), HNC-B (green diamonds), and HNC-C (red squares) samples. Symbol sizes are larger than or comparable to the experimental errors. The solid lines are the best fits using eqs 1 and 3, when using $\tau_{core}^{LT}(B)$, the extracted normalized exchange energies (χ), and $\gamma_b = \tau_{core}^{RT}/\tau_{cs}^{RT}$ values (see text). (b) The blue symbols represent the obtained $\Delta_{bd} = 3\eta$ values which determine the magnetic field dependent lifetimes of panel a. The green symbols correspond to the energy values of Δ obtained by fitting the *T*-dependence of the PL lifetimes (solid curves in Figure 2c) to eq 3. The blue dashed-line represents the theoretical volume-dependence of $\Delta_{bd} \propto R^{-3}$ for type-I CdTe-QDs.[5,6,20,27] The green dotted-line shows the volume-dependence of the lowest-energy acoustic phonon mode (l = 2; $\Delta_{AP} \propto R^{-1}$) for isolated CdTe spheres, computed from Lamb's theory.[29,41,42]

DOI: 10.1021/acsnano.5b07158
ACS Nano 2016, 10, 4102−4110

sample, the lifetime decreases with $1/\zeta^2$ until it levels off at high fields when the Zeeman energy is comparable to or larger than the exchange energy. This typical magnetic field dependence gradually disappears with decreasing exchange energy, until for sample HNC-B (V_{HNC} = 80 nm^3, V_{CdSe} = ~70.8 nm^3 and χ = 0.067) the effective lifetime is short and independent of field, because already at low magnetic fields the Zeeman energy exceeds the exchange energy. These results show that eq 3 describes the proper behavior of the dark exciton lifetimes of type-I, type-I$^{1/2}$, or quasi-type-II and type-II NCs as a function of magnetic field strength, confirming the consistency of our approach.

***T*-Dependence of the Exciton Lifetime: Bright−Dark Splitting *versus* Acoustic Phonon Energy.** In our model (eq 3), the *T*-dependence of the PL decay times is fully determined by the energy splitting Δ in the Boltzmann distribution. The model neglects phonon-assisted transitions, the influence of higher lying exciton levels, and assumes that this energy level structure works for both direct and indirect excitons. Using a simple Boltzmann distribution assumes that the relaxation from the higher exciton levels to the lowest dark one is sufficiently fast to equilibrate the levels. In a first attempt to describe the *T*-behavior of all samples (Figure 2c), we use $\Delta = \Delta_{bd}$, the bright−dark splitting.[2] We assume the bright−dark energy splitting to scale as $\Delta_{bd} \simeq 3\eta_{cs}$,[6,27] resulting in Δ_{bd} energies shown by the blue symbols in Figure 5b. The blue dashed line corresponds to the nominal *R*-dependence of Δ_{bd} for a CdTe type-I NC.[5,20,27] Inserting these Δ_{bd}-values in eq 3 leads to the colored dashed lines in Figure 2c. Some aspects of the data are properly described by the model, where $\chi = \gamma_b$ is assumed (see eq 3 and Figure 4c). By construction, both the low *T* and high *T* limits of the data are in good agreement. The value of the exciton lifetime at low *T*, in the saturation plateau below 4 K, is determined by the competition between effects of e−h overlap and exchange interaction. With increasing shell volume, the exchange interaction reduces, leading to an initial shortening of the lifetime (HNC-A). With further increasing shell volume, the e−h overlap is reduced to such an extent that the oscillator strength significantly drops, leading to an increase of the lifetime (HNC-B). At high *T*, the calculated exciton lifetime is only determined by the e−h overlap, leading to a prolonged lifetime with increasing shell volume. The minor drop in lifetime with *T* observed for the type-II system (HNC-B) is well described by the model. In contrast, for the core-only and HNC-A sample only qualitative agreement is obtained: the model overestimates the temperature at which the lifetime suddenly drops (end of plateau, 20 *versus* 4 K for core-only sample, 10 *versus* 4 K for sample HNC-A). These observations are in agreement with previous experiments on nearly spherical type-I CdSe NCs[2] (see also Figure S7 for an extended discussion). Furthermore, the slight increase of the lifetime of sample HNC-A at elevated temperatures (above 100 K) cannot be explained by the model and is possibly due to the effect of higher lying exciton levels.

Better quantitative agreement for all samples is obtained by using Δ as a fitting parameter (solid lines in Figure 2c), resulting in Δ-values significantly smaller than Δ_{bd}, shown by the green symbols in Figure 5b. These smaller energies are comparable to the typical energies of acoustic phonon (AP) modes,[37] as indicated by the green dotted-line in Figure 5b, which shows the calculated lowest-energy breathing mode for isolated CdTe spherical QDs. Its energy scales weakly with the overall NC size as $\Delta_{AP} \propto R^{-1}$.[29,41,42] These results strongly suggest that acoustic phonons are involved in the exciton recombination,[29] in agreement with single dot measurements,[19,39,43] a recent fluorescence line narrowing experiment on CdSe/CdS dot-in-rod HNCs[37] and *T*-dependent lifetime measurements on ZnSe QDs.[30] Emission of acoustic phonons elastically distort the NCs, resulting in an additional mixing between bright and dark levels, leading to a reduction of the dark exciton lifetime.[30,37,44,45] The difference between Δ_{AP} and Δ_{bd} is particularly large for type-I and quasi-type-II or type-I$^{1/2}$ structures, whereas for sample HNC-B, both energies are comparable. In that case, both the Δ_{AP} and Δ_{bd} models show an exciton lifetime that is relative insensitive to temperature (dashed green line in Figure 2c), which is characteristic for a type-II system.

CONCLUSION

We have presented a method to determine the electron−hole exchange energy η of core−shell HNCs by measuring the PL decay times in strong magnetic fields. The method relies on normalizing the field-dependent lifetime of a core−shell nanocrystal to that of the core-only sample and using an analytic expression of the exciton lifetime in the effective-mass approximation that includes η as a parameter. We have found that the exchange energy of CdTe/CdSe HNCs with variable shell thickness scales linearly with the electron−hole overlap, determined independently within a RT lifetime experiment. The ability to independently determine e−h overlap and e−h exchange permits us to unravel their effects on the exciton lifetime of HNCs. We find that the dark exciton lifetime scales with η, whether η is varied by NC size (with η) or by e−h overlap (with η^2). Both bright and dark exciton lifetimes are inversely proportional to the e−h overlap. Our findings result in a comprehensive model that explains the exciton PL decay time as a function of all relevant experimental parameters, such as core radius, core/shell volume, shell volume fraction, magnetic field strength, and temperature. This description shows that, unlike type-I NCs with a large e−h overlap, type-II structures exhibit a weak exchange interaction, resulting in exciton lifetimes that are remarkably constant with both temperature and magnetic field strength. The full temperature dependence of HNCs can, however, only be described when acoustic phonon assisted emission is involved in the radiative emission. The formula we propose is defined in general terms and can be used for type-I, quasi-type-II or type-I$^{1/2}$, and type-II semiconductor nanocrystals and is valid for different material systems.

METHODS

Heteronanocrystal Synthesis. The high-quality colloidal CdTe/CdSe HNCs were synthesized and described in detail by Chin *et al.*[8] These samples were extensively investigated and characterized by X-ray diffraction, high resolution electron microscopy, and optical spectroscopy.[8,10]

Temperature-Dependence of the PL Decay Times. PL decay curves were obtained by using a picosecond diode pulse laser, operating at 406 nm. The repetition rates (0.2−20 MHz) were controlled by the laser driver internal clock or using an internal pulse generator. Very low excitation fluences were used (0.5 nJ/cm^2) in order to avoid multiexciton formation, and to keep the ratio of stop to start pulses below 0.04. The PL was filtered through a crossed polarizer and a combination of suitable optical cutoff filters to eliminate scattered laser light, dispersed by a 0.1 m monochromator (1350 lines/mm grating, blazed at 500 nm) and detected by a fast photomultiplier tube (PMT). The PL decay curves were obtained by a

DOI: 10.1021/acsnano.5b07158
ACS Nano 2016, 10, 4102−4110

single-photon counter (time-correlated single photon counting), while monitoring the PL peak wavelength. The samples were contained in a sealed quartz cuvette (optical path: 3 mm) and mounted in a continuous He-flow cryostat allowing for measurements down to 1.2 K. The experimental setup has been described before.[3,10]

Optical Measurements in High-Magnetic Fields. Optical experiments at low temperatures and high magnetic fields were performed on a set of NC ensemble samples, using two spectroscopic techniques: steady-state photoluminescence (PL) and time-resolved PL (trPL). For the optical experiments, diluted HNCs solutions were drop-casted on Si/SiO_2 substrates in which the HNC ensembles are randomly oriented. The NC samples were mounted in a titanium sample holder on top of a three-axis piezo-positioner. The sample stage was placed in a homemade optical probe, made of carbon and titanium to minimize possible displacements at high magnetic fields. Laser light was focused on the sample by a singlet lens (10 mm focal length). The same lens was used to collect the PL emission and direct it to the detection setup (Backscattering geometry). The optical probe was mounted inside a liquid helium bath cryostat (4.2 K) inserted in a 50 mm bore Florida-Bitter electro-magnet with a maximum field strength of 31 T. All optical experiments were performed in Faraday geometry (light excitation and detection parallel to the magnetic field direction).

For trPL measurements, the excitation was provided by a picosecond pulsed diode-laser operating at 406 nm. The same repetition rate (125 kHz) was used for all samples and controlled by the laser driver internal clock. Very low excitation fluences were used in order to avoid multiexciton formation, and to keep the ratio of stop to start pulses below 0.02. The very low repetition rates ensure that in each laser-pulse less than one exciton is promoted in the NC at the time. The PL decay signal of each individual sample was filtered by long and short-pass filters, with a bandwidth of about ±30 nm at the center of the PL spectral postion. The PL signal was detected by an avalanche photo diode connected to a single-photon counter (time-correlated single photon counting). For static, spectrally resolved PL measurements, the excitation source was the 476.5 nm line of an argon-ion laser. The PL light was guided through a 300 mm long single grating spectrometer (300 or 150 grooves/mm grating) and detected by a liquid nitrogen cooled charge couple device (CCD). Cut-off optical filters were used in excitation and detection, for both PL and trPL experiments.

PL Decay Times Analysis. Biexponential or also multiexponential behavior is typical for the PL decay curves of NCs ensembles. To ensure consistent comparison between the different samples and the various experiments, the raw PL decay curves were background subtracted and fitted to a single-exponential function. The analysis was performed at the end part of the decay curves, where the intensity signal is less than 5−10% of the initial intensity at $t = 0$. The extracted PL lifetime is assigned to exciton radiative recombination (see Figure S3). This is a common procedure in the derivation of exciton (PL) lifetimes in semiconductor NCs.[2,20]

ASSOCIATED CONTENT

Supporting Information

The Supporting Information is available free of charge on the ACS Publications website at DOI: 10.1021/acsnano.5b07158.

Additional information including details on data analysis and methods, extra optical spectra and a discussion on the degree of bright−dark exciton mixing for type-II HNCs and on the volume-dependence of the dark exciton lifetime in type-I HNCs (PDF)

AUTHOR INFORMATION

Corresponding Author

*E-mail: P.Christianen@science.ru.nl.

Author Contributions

C.d.M.D. and P.C.M.C. initiated the project. E.G. synthesized and characterized the nanocrystals. A.G.d.A., C.d.M.D., and P.C.M.C. planned the optical experiments. A.G.d.A. and C.d.M.D. performed the optical experiments. A.G.d.A. analyzed the results. A.G.d.A. and P.C.M.C. interpreted the data and wrote the manuscript.

Notes

The authors declare no competing financial interest.

ACKNOWLEDGMENTS

We acknowledge the support of HFML-RU/FOM, member of the European Magnetic Field Laboratory (EMFL). Part of this work has been supported by EuroMagNET II under the EU contract number 228043.

REFERENCES

(1) Norris, D. J.; Efros, A. L.; Rosen, M.; Bawendi, M. G. Size Dependence of Exciton Fine Structure in CdSe Quantum Dots. *Phys. Rev. B: Condens. Matter Mater. Phys.* **1996**, *53*, 16347−16354.

(2) Crooker, S. A.; Barrick, T.; Hollingsworth, J. A.; Klimov, V. I. Multiple Temperature Regimes of Radiative Decay in CdSe Nanocrystal Quantum Dots: Intrinsic Limits to the Dark-Exciton Lifetime. *Appl. Phys. Lett.* **2003**, *82*, 2793−2795.

(3) de Mello Donegá, C.; Bode, M.; Meijerink, A. Size- and Temperature-Dependence of Exciton Lifetimes in CdSe Quantum Dots. *Phys. Rev. B: Condens. Matter Mater. Phys.* **2006**, *74*, 085320.

(4) Valerini, D.; Cretí, A.; Lomascolo, M.; Manna, L.; Cingolani, R.; Anni, M. Temperature Dependence of the Photoluminescence Properties of Colloidal CdSe/ZnS Core/Shell Quantum Dots Embedded in a Polystyrene Matrix. *Phys. Rev. B: Condens. Matter Mater. Phys.* **2005**, *71*, 235409.

(5) Efros, A. L.; Rosen, M.; Kuno, M.; Nirmal, M.; Norris, D. J.; Bawendi, M. Band-Edge Exciton in Quantum Dots of Semiconductors with a Degenerate Valence Band: Dark and Bright Exciton States. *Phys. Rev. B: Condens. Matter Mater. Phys.* **1996**, *54*, 4843−4856.

(6) Zhao, Q.; Graf, P. A.; Jones, W. B.; Franceschetti, A.; Li, J.; Wang; Kim, K. Shape Dependence of Band-Edge Exciton Fine Structure in CdSe Nanocrystals. *Nano Lett.* **2007**, *7*, 3274−3280.

(7) Nirmal, M.; Norris, D. J.; Kuno, M.; Bawendi, M. G.; Efros, A. L.; Rosen, M. Observation of the "Dark Exciton" in CdSe Quantum Dots. *Phys. Rev. Lett.* **1995**, *75*, 3728−3731.

(8) Chin, P. T. K.; de Mello Donegá, C.; van Bavel, S. S.; Meskers, S. C. J.; Sommerdijk, N. A. J. M.; Janssen, R. A. J. Highly Luminescent CdTe/CdSe Colloidal Heteronanocrystals with Temperature-Dependent Emission Color. *J. Am. Chem. Soc.* **2007**, *129*, 14880−14886.

(9) Ivanov, S. A.; Piryatinski, A.; Nanda, J.; Tretiak, S.; Zavadil, K. R.; Wallace, W. O.; Werder, D.; Klimov, V. I. Type-II Core/Shell CdS/ZnSe Nanocrystals: Synthesis, Electronic Structures, and Spectroscopic Properties. *J. Am. Chem. Soc.* **2007**, *129*, 11708−11719.

(10) de Mello Donegá, C. Formation of Nanoscale Spatially Indirect Excitons: Evolution of the Type-II Optical Character of CdTe/CdSe Heteronanocrystals. *Phys. Rev. B: Condens. Matter Mater. Phys.* **2010**, *81*, 165303.

(11) de Mello Donegá, C. Synthesis and Properties of Colloidal Heteronanocrystals. *Chem. Soc. Rev.* **2011**, *40*, 1512−1546.

(12) Brovelli, S.; Schaller, R. D.; Crooker, S. A.; Garcí-Santamarí, F.; Chen, Y.; Viswanatha, R.; Hollingsworth, J. A.; Htoon, H.; Klimov, V. I. Nano-Engineered Electron-Hole Exchange Interaction Controls Exciton Dynamics in Core-Shell Semiconductor Nanocrystals. *Nat. Commun.* **2011**, *2*, 280.

(13) Rainò, G.; Stöferle, T.; Moreels, I.; Gomes, R.; Kamal, J. S.; Hens, Z.; Mahrt, R. F. Probing the Wave Function Delocalization in CdSe/CdS Dot-in-Rod Nanocrystals by Time- and Temperature-Resolved Spectroscopy. *ACS Nano* **2011**, *5*, 4031−4036.

(14) Groeneveld, E.; van Berkum, S.; van Schooneveld, M. M.; Gloter, A.; Meeldijk, J. D.; van den Heuvel, D. J.; Gerritsen, H. C.; de

DOI: 10.1021/acsnano.5b07158
ACS Nano 2016, 10, 4102−4110

Mello Donegá, C. Highly Luminescent (Zn,Cd)Te/CdSe Colloidal Heteronanowires with Tunable Electron-Hole Overlap. *Nano Lett.* **2012**, *12*, 749−757.
(15) Rainò, G.; Stöferle, T.; Moreels, I.; Gomes, R.; Hens, Z.; Mahrt, R. F. Controlling the Exciton Fine Structure Splitting in CdSe/CdS Dot-in-Rod Nanojunctions. *ACS Nano* **2012**, *6*, 1979−1987.
(16) Wei, S.-H.; Zhang, S. B.; Zunger, A. First-Principles Calculation of Band Offsets, Optical Bowings, and Defects in CdS, CdSe, CdTe, and their Alloys. *J. Appl. Phys.* **2000**, *87*, 1304−1311.
(17) Johnston-Halperin, E.; Awschalom, D. D.; Crooker, S. A.; Efros, A. L.; Rosen, M.; Peng, X.; Alivisatos, A. P. Spin Spectroscopy of Dark Excitons in CdSe Quantum Dots to 60 T. *Phys. Rev. B: Condens. Matter Mater. Phys.* **2001**, *63*, 205309.
(18) Furis, M.; Hollingsworth, J. A.; Klimov, V. I.; Crooker, S. A. Time- and Polarization-Resolved Optical Spectroscopy of Colloidal CdSe Nanocrystal Quantum Dots in High Magnetic Fields. *J. Phys. Chem. B* **2005**, *109*, 15332−15338.
(19) Biadala, L.; Louyer, Y.; Tamarat, P.; Lounis, B. Band-Edge Exciton Fine Structure of Single CdSe/ZnS Nanocrystals in External Magnetic Fields. *Phys. Rev. Lett.* **2010**, *105*, 157402.
(20) Blokland, J. H.; Claessen, V. I.; Wijnen, F. J. P.; Groeneveld, E.; de Mello Donegá, C.; Vanmaekelbergh, D.; Meijerink, A.; Maan, J. C.; Christianen, P. C. M. Exciton Lifetimes of CdTe Nanocrystal Quantum Dots in High Magnetic Fields. *Phys. Rev. B: Condens. Matter Mater. Phys.* **2011**, *83*, 035304.
(21) Liu, F.; Rodina, A. V.; Yakovlev, D. R.; Greilich, A.; Golovatenko, A. A.; Susha, A. S.; Rogach, A. L.; Kusrayev, Y. G.; Bayer, M. Exciton Spin Dynamics of Colloidal CdTe Nanocrystals in Magnetic Fields. *Phys. Rev. B: Condens. Matter Mater. Phys.* **2014**, *89*, 115306.
(22) de Mello Donegá, C.; Koole, R. Size Dependence of the Spontaneous Emission Rate and Absorption Cross Section of CdSe and CdTe Quantum Dots. *J. Phys. Chem. C* **2009**, *113*, 6511−6520.
(23) Efros, A. L. Luminescence Polarization of CdSe Microcrystals. *Phys. Rev. B: Condens. Matter Mater. Phys.* **1992**, *46*, 7448−7458.
(24) García-Santamaría, F.; Brovelli, S.; Viswanatha, R.; Hollingsworth, J. A.; Htoon, H.; Crooker, S. A.; Klimov, V. I. Breakdown of Volume Scaling in Auger Recombination in CdSe/CdS Heteronanocrystals: The Role of the Core-Shell Interface. *Nano Lett.* **2011**, *11*, 687−693.
(25) Schaller, R. D.; Crooker, S. A.; Bussian, D. A.; Pietryga, J. M.; Joo, J.; Klimov, V. I. Revealing the Exciton Fine Structure of PbSe Nanocrystal Quantum Dots Using Optical Spectroscopy in High Magnetic Fields. *Phys. Rev. Lett.* **2010**, *105*, 067403.
(26) Chen, P.; Whaley, K. Magneto-Optical Response of CdSe Nanostructures. *Phys. Rev. B: Condens. Matter Mater. Phys.* **2004**, *70*, 045311.
(27) Lavallard, P.; Chamarro, M.; Pérez-Conde, J.; Bhattacharjee, A.; Goupalov, S.; Lipovskii, A. Exchange Interaction and Acoustical Phonon Modes in CdTe Nanocrystals. *Solid State Commun.* **2003**, *127*, 439−442.
(28) Le Thomas, N.; Herz, E.; Schöps, O.; Woggon, U.; Artemyev, M. V. Exciton Fine Structure in Single CdSe Nanorods. *Phys. Rev. Lett.* **2005**, *94*, 016803.
(29) Oron, D.; Aharoni, A.; de Mello Donegá, C.; van Rijssel, J.; Meijerink, A.; Banin, U. Universal Role of Discrete Acoustic Phonons in the Low-Temperature Optical Emission of Colloidal Quantum Dots. *Phys. Rev. Lett.* **2009**, *102*, 177402.
(30) Eilers, J.; van Hest, J.; Meijerink, A.; Donega, C. d. M. Unravelling the Size and Temperature Dependence of Exciton Lifetimes in Colloidal ZnSe Quantum Dots. *J. Phys. Chem. C* **2014**, *118*, 23313−23319.
(31) Leung, K.; Pokrant, S.; Whaley, K. B. Exciton Fine Structure in CdSe Nanoclusters. *Phys. Rev. B: Condens. Matter Mater. Phys.* **1998**, *57*, 12291−12301.
(32) Califano, M.; Franceschetti, A.; Zunger, A. Lifetime and Polarization of the Radiative Decay of Excitons, Biexcitons, and Trions in CdSe Nanocrystal Quantum Dots. *Phys. Rev. B: Condens. Matter Mater. Phys.* **2007**, *75*, 115401.
(33) Kuno, M.; Nirmal, M.; Bawendi, M. G.; Efros, A.; Rosen, M. Magnetic Circular Dichroism Study of CdSe Quantum Dots. *J. Chem. Phys.* **1998**, *108*, 4242−4247.
(34) Kiselev, A. A.; Ivchenko, E. L.; Rössler, U. Electron g factor in One- and Zero-Dimensional Semiconductor Nanostructures. *Phys. Rev. B: Condens. Matter Mater. Phys.* **1998**, *58*, 16353−16359.
(35) Rodina, A. V.; Efros, A. L.; Alekseev, A. Y. Effect of the Surface on the Electron Quantum Size Levels and Electron g factor in Spherical Semiconductor Nanocrystals. *Phys. Rev. B: Condens. Matter Mater. Phys.* **2003**, *67*, 155312.
(36) van Bree, J.; Silov, A. Y.; Koenraad, P. M.; Flatté, M. E.; Pryor, C. E. g factors and Diamagnetic Coefficients of Electrons, Holes, and Excitons in InAs/InP Quantum Dots. *Phys. Rev. B: Condens. Matter Mater. Phys.* **2012**, *85*, 165323.
(37) Granados del Águila, A.; Jha, B.; Pietra, F.; Groeneveld, E.; de Mello Donegá, C.; Maan, J. C.; Vanmaekelbergh, D.; Christianen, P. C. M. Observation of the Full Exciton and Phonon Fine Structure in CdSe/CdS Dot-in-Rod Heteronanocrystals. *ACS Nano* **2014**, *8*, 5921−5931.
(38) He, J.; Zhong, H.; Scholes, G. D. Electron-Hole Overlap Dictates the Hole Spin Relaxation Rate in Nanocrystal Heterostructures. *Phys. Rev. Lett.* **2010**, *105*, 046601.
(39) Labeau, O.; Tamarat, P.; Lounis, B. Temperature Dependence of the Luminescence Lifetime of Single CdSe/ZnS Quantum Dots. *Phys. Rev. Lett.* **2003**, *90*, 257404.
(40) Biadala, L.; Siebers, B.; Gomes, R.; Hens, Z.; Yakovlev, D. R.; Bayer, M. Tuning Energy Splitting and Recombination Dynamics of Dark and Bright Excitons in CdSe/CdS Dot-in-Rod Colloidal Nanostructures. *J. Phys. Chem. C* **2014**, *118*, 22309−22316.
(41) Takagahara, T. Electron-Phonon Interactions in Semiconductor Nanocrystals. *J. Lumin.* **1996**, *70*, 129−143.
(42) Salvador, M. R.; Graham, M. W.; Scholes, G. D. Exciton-Phonon Coupling and Disorder in the Excited States of CdSe Colloidal Quantum Dots. *J. Chem. Phys.* **2006**, *125*, 184709.
(43) Biadala, L.; Louyer, Y.; Tamarat, P.; Lounis, B. Direct Observation of the Two Lowest Exciton Zero-Phonon Lines in Single CdSe/ZnS Nanocrystals. *Phys. Rev. Lett.* **2009**, *103*, 037404.
(44) Wong, C. Y.; Kim, J.; Nair, P. S.; Nagy, M. C.; Scholes, G. D. Relaxation in the Exciton Fine Structure of Semiconductor Nanocrystals. *J. Phys. Chem. C* **2009**, *113*, 795−811.
(45) Huxter, V. M.; Scholes, G. D. Acoustic Phonon Strain Induced Mixing of the Fine Structure Levels in Colloidal CdSe Quantum Dots Observed by a Polarization Grating Technique. *J. Chem. Phys.* **2010**, *132*, 104506.

DOI: 10.1021/acsnano.5b07158
ACS Nano 2016, 10, 4102−4110